CrossMark

Enhanced intracellular translocation and biodistribution of gold nanoparticles functionalized with a cell-penetrating peptide (VG-21) from vesicular stomatitis virus

Pooja Munnilal Tiwari [a], Erdal Eroglu [a, b], Swapnil Subhash Bawage [a], Komal Vig [a], Michael E. Miller [c], Shreekumar Pillai [a], Vida A. Dennis [a], Shree Ram Singh [a, *]

[a] Center for NanoBiotechnology Research and Department of Biological Sciences, Alabama State University, 1627 Hall Street, Montgomery, AL 36101, USA
[b] Faculty of Engineering, Bioengineering Department, Celal Bayar University, 45140 Muradiye, Manisa, Turkey
[c] Auburn University Research Instrumentation Facility, Harrison School of Pharmacy, 32 Rouse Life Sciences Building, Auburn University, Auburn, AL 36849, USA

ARTICLE INFO

ABSTRACT

Reduced toxicity and ease of modification make gold nanoparticles (GNPs) suitable for targeted delivery, bioimaging and theranostics by conjugating cell-penetrating peptides (CPPs). This study presents the biodistribution and enhanced intracellular uptake of GNPs functionalized with VG-21, a CPP derived from vesicular stomatitis virus glycoprotein (G). Cell penetrating efficiency of VG-21 was demonstrated using CellPPD web server, conjugated to GNPs and were characterized using, UV-visible and FTIR spectroscopy, transmission electron microscopy, dynamic light scattering and zeta potential. Uptake of VG-21 functionalized GNPs (fGNPs) was tested in eukaryotic cell lines, HEp-2, HeLa, Vero and Cos-7, using flow cytometry, fluorescence and transmission electron microscopy (TEM), and inductively coupled plasmon optical emission spectroscopy (ICP-OES). The effects of nanoparticles on stress and toxicity related genes were studied in HEp-2 cells. Cytokine response to fGNPs was studied in vitro and in vivo. Biodistribution of nanoparticles was studied in BALB/c mice using TEM and ICP-OES. VG-21, GNPs and fGNPs had little to no effect on cell viability. Upon exposure to fGNPs, HEp-2 cells revealed minimal down regulation of stress response genes. fGNPs displayed higher uptake than GNPs in all cell lines with highest internalization by HEp-2, HeLa and Cos-7 cells, in endocytotic vesicles and nuclei. Cytokine ELISA showed that mouse J774 cells exposed to fGNPs produced less IL-6 than did GNP-treated macrophage cells, whereas TNF-α levels were low in both treatment groups. Biodistribution studies in BALB/c mice revealed higher accumulation of fGNPs than GNPs in the liver and spleen. Histopathological analyses showed that fGNP-treated mice accumulated 35 ng/mg tissue and 20 ng/mg tissue gold in spleen and liver respectively, without any adverse effects. Likewise, serum cytokines were low in both GNP- and fGNP-treated mice. Thus, VG-21-conjugated GNPs have enhanced cellular internalization and are suitable for various biomedical applications as nano-conjugates.

1. Introduction

To achieve enhanced and targeted delivery of biomolecules, several delivery vehicles have been developed including nanoparticles. Despite their versatility, metal nanoparticles face challenges including toxicity, inefficiency in translocation into cells and clearance from tissues or organs. To overcome many of these barriers, gold nanoparticles (GNPs) have been employed [1,2]. GNPs, functionalized with nucleic acids, drugs, antibodies, PEG [3], siRNA [3,4] or peptides [5,6], have exhibited low cytotoxicity and excellent biodistribution abilities [2]. These functionalized GNPs (fGNPs) are used for gene transfection and silencing, targeted drug or gene delivery [5], intracellular detection, bioimaging [7], cancer studies [8,9] and as biosensors [10]. Among these fGNPs, peptide conjugated GNPs have been used routinely for enhanced cell penetration efficiency.

Most commonly used peptides for conjugation with GNPs are the cell penetrating peptides (CPPs). CPPs are short peptides with membrane translocation capability and are widely used for delivery of therapeutic molecules, proteins, liposomes, nanoparticles, antisense molecules, siRNA and nucleic acids [11]. CPPs usually translocate through biological membranes via direct penetration,

* Corresponding author. Tel.: +1 334 229 4168.
E-mail address: ssingh@alasu.edu (S.R. Singh).

formation of inverted micelles or transient pores, macropinocytosis [12], clathrin or caveolae-mediated endocytosis [13] or micropinocytosis [14]. Most commonly used CPPs include those from nuclear localization signals and protein transduction domains of viruses, amphipathic peptides and arginine rich peptides [12]. The most commonly used CPP is the commercially available HIV TAT (protein trans-activator of transcription) peptide [6,15] for delivery of macromolecules and/or drugs into the nucleus or cytoplasm. Other CPPs employed for enhanced delivery purposes are human surfactant protein B (a lung surfactant), orexin (a neuropeptide hormone) and lactoferricin (a globular glycoprotein) [16], a secondary amphipathic CPP (named CADY) [17], malittin derived peptide [4], Rev peptide (from HIV-1 regulatory protein) [18], CALNNR$_8$ [19] and GC rich peptide with RGD [20] and flock house virus derived CPP [21].

GNPs functionalized with CPPs translocate to the cytoplasm and the nucleus [22]. Thus, the rationale behind our study was to develop a combination of these CPPs and GNPs to provide nanovectors for delivery of biomolecules with enhanced cellular uptake. We have designed a similar peptide, VG-21, from the vesicular stomatitis virus (VSV) glycoprotein G (VSV-G). VSV is a rhabdovirus with a non-segmented, negative, single-strand RNA genome, known to have oncolytic activity against various cancers [23–26]. VSV-G recognizes the receptors on the host cell membrane and mediates endocytosis of the virion into cells, followed by membrane fusion through structural rearrangement [27]. VSV-G has been shown to translocate through the stacks of Golgi without leaving the cisternal lumen and without entering the Golgi vesicles [28]. Due to its inherent properties of membrane fusion, translocation and ability to enhance the transfection efficiency, VSV-G has been used for pseudotyping of the viruses and developing recombinant gene transfer vectors, especially in conjunction with the lentiviral vectors [29–32].

For the first time, we have designed a CPP (VG-21) from VSV-G and evaluated its potential for enhanced delivery of GNPs. First, we functionalized GNPs with VG-21 (fGNPs), followed by characterization and evaluation as an intracellular delivery system. We have also evaluated the efficiency of these VG-21 fGNPs in vitro in four mammalian cell lines (HEp-2, HeLa, Vero and Cos-7) and in vivo in mice. We hypothesized that VG-21 would enhance the translocation efficiency of GNPs. In addition, we also evaluated the interaction of fGNPs with HEp-2 cells by assessing their impact on stress response genes. Similarly, the impact of fGNPs on cytokine production was studied in J774 mouse macrophage cells using ELISA. Finally, we analyzed the translocation efficiency and biodistribution of these VG-21 fGNPs in comparison to GNPs in mice.

2. Materials and methods

2.1. Peptide characterization

VG-21 peptide derived from VSV-G protein was first evaluated for cell penetrating efficiency. The support vector machine (SVM) based cell penetrating peptide prediction was performed with CellPPD web server which predicts efficient cell penetrating peptides [33]. The SVM + Motif prediction method was selected at an SVM threshold of −0.1 and a motif e-value of 10. The three dimensional structure of VG-21 was elucidated using peptide tertiary structure prediction server, Pepstr, which allows modeling of small peptides (7–25 amino acid residues) [34]. The Pepstr server then refines the modeled structure with energy minimization and molecular dynamic simulations. The structure was validated with VADAR (Volume Area Dihedral Angle Reporter) web server [35] and analyzed with RasWin and Molegro molecular viewer. The energy map and surface electrostatics of the peptide were analyzed using Molegro molecular viewer.

2.2. Nanoparticle functionalization and characterization

Carboxyl-polymer coated spherical GNPs (Nanopartz™, Loveland, CO, USA) 13 nm in size, were functionalized with VG-21 peptide (Bachem Americas Inc., Santa Clara, CA, USA) using 1-Ethyl-3-(3-dimethylaminopropyl)carbodiimide (EDC, Sigma Aldrich, St. Louis, MO, USA) chemistry. Briefly, the GNPs were mixed with peptide (17 μM) and EDC and vortexed for an hour. The peptide concentration was kept higher than the number of free carboxyl groups on the GNPs. Unbound peptide was removed by repeated centrifugation at 18000× g for 50 min and the GNPs were finally re-suspended in sterile deionized water up to 1 ml. Functionalization was assessed using UV–Vis spectrophotometry (Beckman Coulter spectrophotometer, Brea, CA, USA) and FTIR spectroscopy. FTIR spectra were collected for GNPs and fGNPs with an FTIR Nicolet 6700 (Thermo Fisher Scientific Inc., Waltham, MA, USA) equipped with an attenuated total reflectance (ATR) stage, with over 128 scans per sample with a resolution of 4 cm^{-1}; background spectra were automatically subtracted.

For TEM analysis, nanoparticles were dropped on carbon coated formavar grid and air dried, prior to observation under the Zeiss EM10 microscope (Carl Zeiss Meditec, Oberkochen, Germany). DLS measurements (size and zeta potential) of nanoparticles were done by a Malvern ZS Nano instrument (Malvern Instruments Westborough, MA, USA).

2.3. Cell viability assay

Human epidermoid type-2 (HEp-2) cells, African green monkey kidney (Vero and Cos-7) and human cervical cancer (HeLa) cell lines (American Type Culture Collection, Manassas, VA, USA) were propagated by standard methods using minimum essential medium (MEM) supplemented with 10% fetal bovine serum (FBS), 2 mM L-glutamine, 75 U/ml penicillin, 100 μg/ml kanamycin and 75 μg/ml streptomycin. The cytotoxicity of GNPs, peptides and functionalized GNPs was determined by MTT (3-(4, 5-dimethyl-thiazol-2-yl)-2,5-diphenyl-tetrazolium bromide) dye reduction assay using CellTiter 96® Non-Radioactive Cell Proliferation Assay (MTT) kit (Promega, Madison, WI, USA). 96-well plates were seeded at 17,000 cells per well in MEM containing 10% FBS and grown overnight. Subsequently, nanoparticles at different concentrations were added to the cells. Cell toxicity was assessed at 24 and 48 h post-incubation with nanoparticles using the MTT assay per the manufacturer's instructions. The absorbance was then measured at 570 nm using a microplate reader (Tecan™ Instruments, San Jose, CA, USA).

2.4. Cellular uptake studies

2.4.1. Fluorescence microscopy

For fluorescence microscopy, FITC conjugated VG-21 peptide was used for functionalization. Cells were plated in 8 chambered slides at 27,000 cells/ well concentration. All cell types were incubated with GNPs and fGNPs for 48 h and fixed in paraformaldehyde-glutaraldehyde, followed by washing with PBS. Nuclei were stained using DAPI and cell membranes were stained using CellMask™ (Life Technologies, Carlsbad, CA, USA). The cells were then imaged using the DAPI, FITC and TRITC channel of the Nikon Ti Eclipse fluorescence microscope (Nikon Inc. Melville, NY, USA).

2.4.2. Flow cytometry

GNPs functionalized with FITC-conjugated VG-21 were used to study internalization of the nanoparticles by flow cytometry. All cells were seeded at 2×10^5 cells per well and incubated overnight at 37 °C with 5% CO$_2$, followed by nanoparticle treatment (1 nM) with an additional incubation for 48 h. These conditions were kept identical for all other experiments unless stated otherwise. Cells were then dissociated, suspended in MEM with no FBS and analyzed with 20,000 events acquired using a BD Canto II FACS instrument (BD Biosciences, San Jose, CA, USA) using the FITC channel. Cells without nanoparticle treatment were used as controls.

2.4.3. Inductively coupled plasmon optical emission spectroscopy (ICP-OES)

Cells were incubated with 1 nM nanoparticles for 48 h, collected and neutralized in concentrated nitric acid for 5 min on a heating block, followed by ICP-OES analysis (Perkin Elmer Optima 7300 V HF version, MA, USA). The measurements were performed against gold standard of 1 mg/L.

2.5. Intracellular translocation studies using transmission electron microscopy (TEM)

Cells were plated and incubated with GNPs and fGNPs for 48 h. Later, the cells were collected, fixed in glutaraldehyde-paraformaldehyde and osmium tetroxide, dehydrated through a graded ethanol series to 100% and polymerized in Embed812 resin. Ultrathin sections were collected on copper grids, stained and then imaged using a Zeiss EM10 TEM microscope.

2.6. Effect of nanoparticles on expression of stress and toxicity related genes in HEp-2 cells

HEp-2 cells were treated with GNPs and fGNPs for 48 h, followed by RNA extraction, cDNA synthesis and qPCR for human stress and toxicity genes using polymerase chain reaction (PCR) array (SA Biosciences, Qiagen, Valencia, CA, USA) which included 84 stress related genes. The results were analyzed using the SA Biosciences online PCR array analysis tool.

2.7. Cytokine production analysis

HEp-2 and J774 mouse macrophage cells were seeded at 2×10^5 cells and 3×10^6 cells per well respectively in 12-well cell culture plate. Cells were then treated with nanoparticles (1 nM) for 24 and 48 h. LPS (50 ng/ml) was used as the positive control. Culture supernatants were collected and tested for cytokine levels for TNF-α and IL-6 using the human and mouse cytokine analysis kit by BD Biosciences per the manufacturer's instructions.

2.8. Biodistribution of GNPs and fGNPs in vivo

Animal experiments were performed according to the National Institutes of Health (NIH) guidelines for animal use and were approved by Alabama State University's Institutional Animal Care and Use Committee (IACUC). Healthy female 4 to 6 week-old BALB/c mice (Charles River Laboratories Inc, Wilmington, MA, USA) were housed under standard approved conditions and provided daily with sterile food and water *ad libitum*.

The study was conducted with four groups of three mice each. Mice were injected intravenously with a low dose 63.72 μg (in 200 μl) or high dose 79.65 μg (in 250 μl) of nanoparticles (GNPs or fGNPs), through their tail veins. Control group of mice were injected with sterile PBS. After 2 days, the animals were sacrificed through CO_2 asphyxiation. Blood and vital organs including lung, liver, heart, kidney, spleen, muscles and brain were collected and stored appropriately until further analyses. The tissues were used for ICP-OES, TEM analysis and histopathology. For quantification of gold in mice, tissue sections were weighed and digested in concentrated nitric acid and analyzed. Uptake of gold was measured per mg of tissues. Similarly, mice tissues with high amounts of gold uptake were chosen for tissue sectioning for TEM and imaged from several fields following same protocol as that used for cells.

2.9. Histopathology

Tissues were fixed in formalin and sent to Nationwide Histology reference laboratory (Spokane, WA, USA). Briefly, tissues were sectioned and stained with hematoxylin and eosin. The images were taken with a Canon EOS digital camera on a Zeiss Axiostar microscope. The histology slides were read by a blinded professional and scored for pathological adversaries.

2.10. Statistical analysis

All the results were analyzed using GraphPad™ Prism software (La Jolla, CA, USA) and presented as ±standard error of means. All the results were subjected to two-way ANOVA and Bonferroni's posttest was applied wherever applicable. The differences were significant at $p < 0.0001$ (***), $p < 0.01$ (**) or $p < 0.05$ (*).

3. Results

3.1. CPP prediction of VG-21 peptide

First, we identified a 21 amino acids long peptide sequence from the VSV G-protein and characterized it for cell penetrating efficiency. VG-21 has 4 negatively charged and 1-positively charged amino acid, with a pI of 4 and was observed to be stable (instability index −24.11) as per the ProtParam analysis [36]. Taking into consideration the amino acid composition and sequence arrangement of the peptide (Fig. 1A), its physicochemical properties like
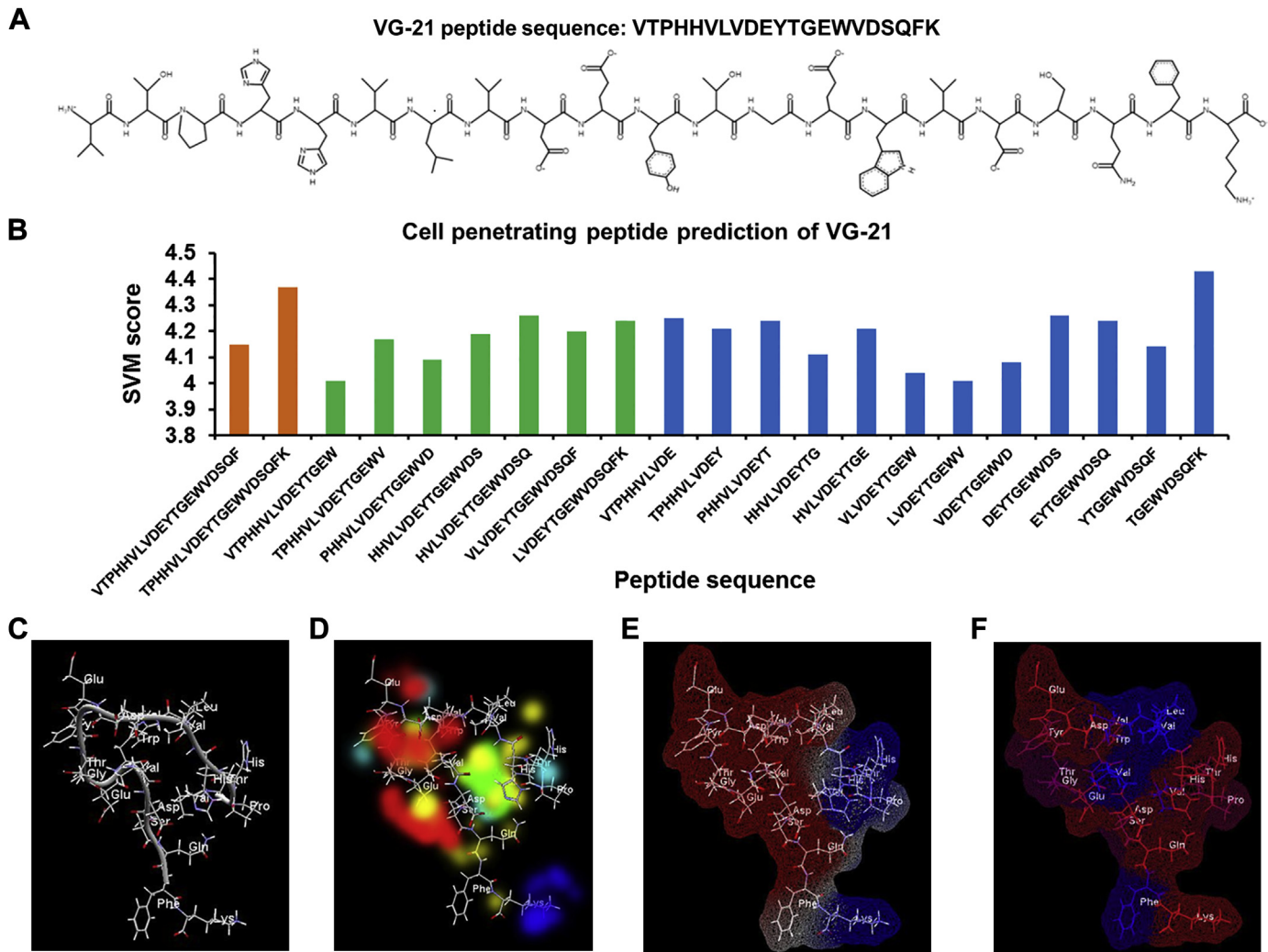

Fig. 1. CPP prediction of VG-21 and three dimensional characterization. (A) sequence and primary structure of VG-21 peptide, (B) SVM score of the CPP predicted motifs (orange, green and blue bars represent 20, 15 and 10 amino acid fragments, respectively), (C) 3-D structure of VG-21, (D) green color represents steric favorable region, blue color represents hydrogen acceptor favorable, red color represents electrostatic, yellow color represents hydrogen donor favorable region associated with VG-21, (E) surface distribution of electrostatic charge, (F) surface hydrophobicity. (For interpretation of the references to color in this figure legend, the reader is referred to the web version of this article.)

hydrophobicity, stearic hindrance, side bulk, hydropathicity, amphipathicity, hydrophilicity, net hydrogen, charge, pI and molecular weight were determined (Supplementary Material S1). CellPPD predicted VG-21 as a CPP along with all the possible 10, 15 and 20 residue long motifs scanned within this peptide (Fig. 1B). The three dimensional structure of VG-21 peptide had a knob like structure, which displayed electrostatic surface distribution, hydrogen exchange (acceptor–donor favorable) space and hydrophobicity associated with the VG-21 peptide (Fig. 1C–F). Upon careful consideration of its charge, water solubility, structure, CPP properties and function in silico, the VG-21 was functionalized onto the GNPs.

3.2. Peptide and GNP conjugation

To confirm functionalization, nanoparticles were characterized using UV–Vis and FTIR spectroscopy. As the size of GNPs and the length of CPP are inversely related to the extent of stability of GNPs [19], we selected 13 nm (±2 nm diameter) carboxylated GNPs and 21 amino acid peptide for this study. GNPs were functionalized with VG-21 using EDC with a molar excess of VG-21 to quench free carboxyl groups of GNPs. The UV–Vis spectra of GNPs shifted from

520 nm to 517 nm indicating the functionalization of GNPs [37] (Fig. 2A). FTIR showed peaks between 2000 and 2500 cm^{-1} that confirmed the conjugation of peptide to GNPs (Fig. 2B). In particular, appearance of bands at 1217, 1364 and 1732 cm^{-1} and a considerable reduction of bands located at 2332 and 2361 cm^{-1} were observed. Characteristic differences were observed between spectra in the 1800–1100 cm^{-1} range, thus affirming successful conjugation [38].

To assess the stability of the conjugates, zeta potential and poly-dispersity were measured at 25 °C using a dynamic light scattering (DLS) system, with sterile distilled water as dispersant. The zeta potential and size measurements also confirmed the functionalization of GNPs wherein the zeta potential of GNPs changed from −53.34 mV to −38.36 mV and hydrodynamic diameter of the GNPs changed from 58.29 nm to 88.40 nm after functionalization with VG-21 (Fig. 2C). Also, the poly-dispersity index of the GNPs changed from 0.14 to 0.25. TEM images of GNPs and VG-21 conjugated GNPs are shown in Fig. 2D. The nanoparticle conjugates were stable for more than a month at 4 °C with minute aggregates which segregated with gentle vortexing, thus depicting the reversible nature of the nanoparticle clusters [39].
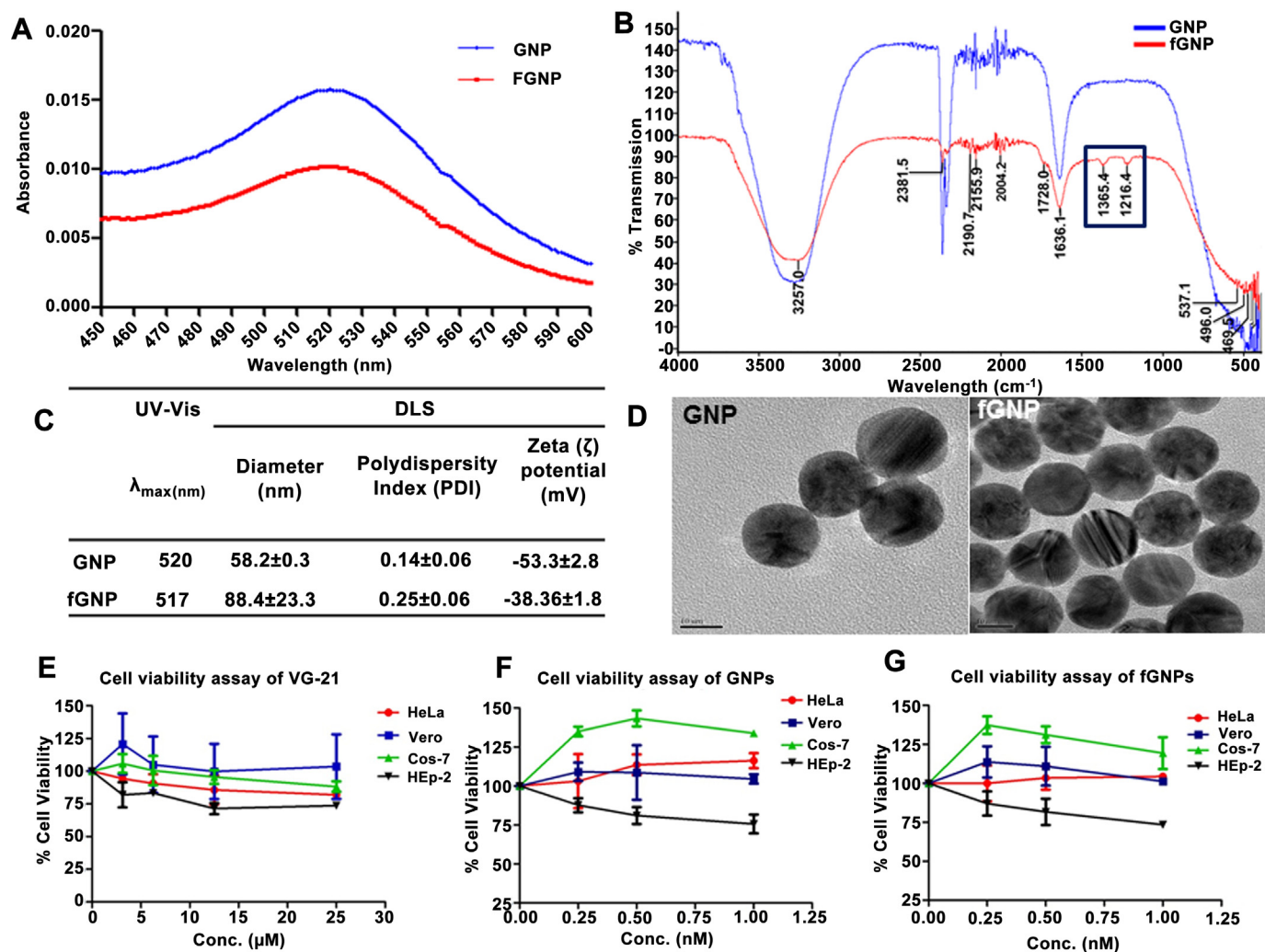

Fig. 2. Characterization of GNPs and fGNPs. UV–Vis spectra of GNPs and fGNPs (A), FTIR spectra of GNP and fGNPs with additional peaks at 1365 cm^{-1} and 1216.4 cm^{-1} appearing for fGNPs (B), DLS characterization for GNPs before and after functionalization (C), TEM images of GNPs and fGNPs (D), Cell viability assay of VG-21 (E), GNPs (F), and fGNPs (G). For VG-21 treatment cell viability for HeLa and Cos-7 cells was 82% and 88% whereas for HEp-2 cells showed 74% viability as compared to Vero cells with no cytotoxicity (100% viability). GNPs and fGNPs at 1 nM showed 100% viability to Vero, HeLa and Cos-7 cells compared with HEp-2 cells exhibiting 75% and 73% viability for GNPs and fGNPs respectively.

3.3. Functionalization of GNPs with VG-21 does not affect cell viability

GNPs and fGNPs were evaluated for their effects on cell viability on HEp-2, HeLa, Vero and Cos-7 cells (Fig. 2E–G). We did not observe any severe cytotoxicity of the peptide, GNPs or fGNPs on any of the cell lines tested by MTT assay. Upon treatment with VG-21, HeLa and Cos-7 cells had 82% and 88% viability whereas HEp-2 cells showed 74% viability as compared to Vero cells with no cytotoxicity (100% viability). GNPs and fGNPs at 1 nM showed no cytotoxicity to Vero, HeLa and Cos-7 cells compared with HEp-2 cells exhibiting 75% and 73% viability respectively.

3.4. Cellular uptake of VG-21 (FITC) functionalized GNPs

After 48 h of treatment with GNPs and fGNPs, HEp-2, HeLa, Vero and Cos-7 cells were assessed for nanoparticle uptake using fluorescence microscopy (Fig. 3A). The cells were stained with nuclear and cell membrane dyes, followed by fixation and imaging using fluorescence microscopy. Fig. 3A shows internalization of fGNPs by all cell lines. The qualitative observations of fluorescence microscopy were reinforced by flow cytometry analysis (Fig. 3B). HeLa and HEp-2 cells expressed higher percentage of FITC-positive cells

at 43.8% and 35.3% respectively, as compared to Vero and Cos-7 cells at 32.4% and 26.6% respectively.

3.5. VG-21 enhances uptake of GNPs in various cell lines

The amount of GNPs and fGNPs internalized by the cells was quantified by ICP-OES. The GNPs internalized was less than that of fGNPs (Fig. 3C). The GNP uptake for HEp-2, HeLa, Vero and Cos-7 cells were 0.3 μg/ml, 0.8 μg/ml, 0.2 μg/ml and 0.3 μg/ml, respectively. The fGNP uptake accounted for 1.4 μg/ml, 1.3 μg/ml, 0.9 μg/ml and 1.3 μg/ml for HEp-2, HeLa, Vero and Cos-7 cells, respectively. We detected significantly higher levels of gold in fGNP treatment in comparison to the GNP-treatment in all cell lines especially HEp-2 and Cos-7 cells (***$p < 0.001$).

3.6. fGNPs and GNPs are localized in endocytotic vesicles and nucleus

The uptake of GNPs and fGNPs were also confirmed by TEM in HEp-2, HeLa, Vero and Cos-7 cells (Fig. 4A–D). GNPs and fGNPs were localized mostly in the endocytotic vesicles. However, some were localized in the nucleus as well as in other cytoplasmic organelles. With the exception of a few cells, GNPs were not detected in large numbers in Cos-7 cells.
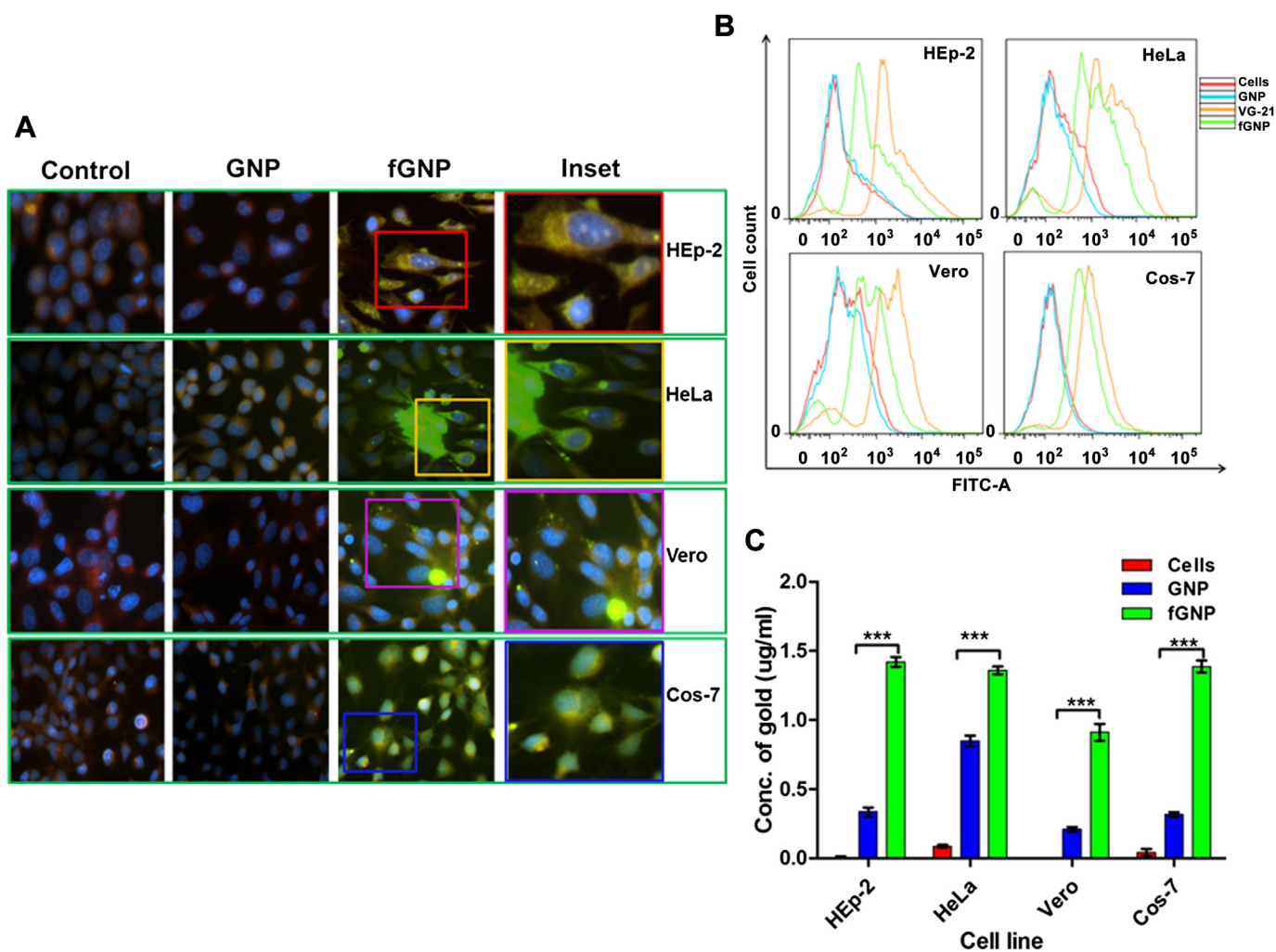

Fig. 3. Cellular uptake of nanoparticles by HEp-2, HeLa, Vero and Cos-7 cell lines. Uptake of nanoparticles was evaluated by Fluorescence microscopy (A), flow cytometry (B) and by ICP-OES (C). In Fig. 3A insets of each fGNP treated cell line images are represented by a different color (Red for HEp-2, gold for HeLa, purple for Vero and blue for Cos-7 cells). Asterisks in panel C indicate significance differences (***$p < 0.001$) of fGNP-treated cells as compared to GNP-treated cells for all cell lines as determined using the Bonferroni posttest. (For interpretation of the references to color in this figure legend, the reader is referred to the web version of this article.)
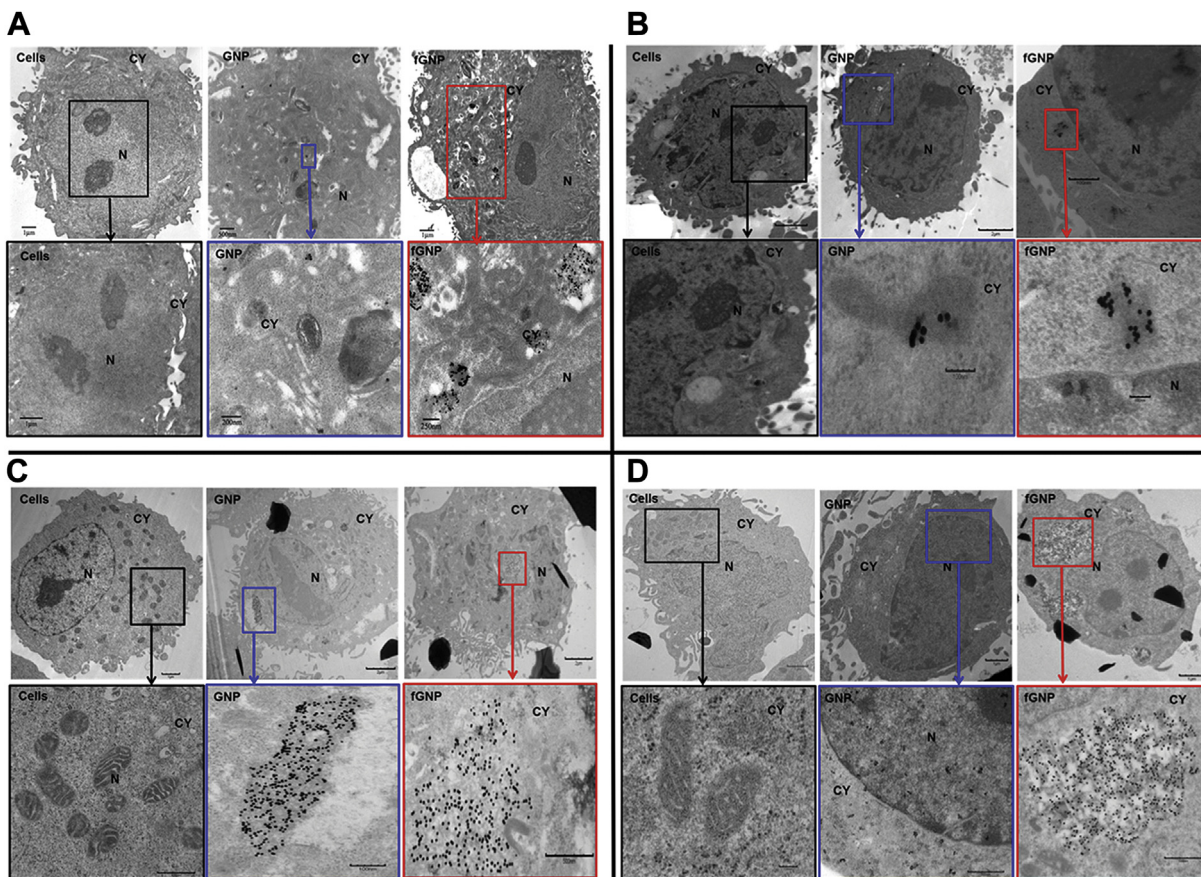
Fig. 4. Cellular uptake of GNPs and fGNPs by HEp-2 (A), HeLa (B), Vero (C) and Cos-7 (D) cells. Each panel represents untreated cells, GNP and fGNP treated cells; N-Nucleus, CY-Cytoplasm. Insets are magnified below each image highlighted with respective colored box (Black for untreated cells, blue for GNP and red for fGNPs). (For interpretation of the references to color in this figure legend, the reader is referred to the web version of this article.)

3.7. VG-21 GNPs induce changes in expression of stress response genes in HEp-2 cells

We evaluated the effects of GNPs and fGNPs on HEp-2 cells with respect to stress response genes. The expression of the genes involved in stress and toxicity was normalized to house-keeping genes in untreated versus GNP or fGNP treated cells. Stress response genes were mostly down-regulated in both GNPs and fGNPs treated cells (Table 1 and Supplementary Material S2). However, the down-regulation levels were lower in fGNPs than in GNPs alone substantiating that masking of GNP surface affects the behavior of host cells. The genes that were relatively more perturbed upon GNP treatment were those involved in the oxidative stress (peroxiredoxin and sequestosome) and hypoxia (matrix metallopeptidase 9), osmotic stress (Aldo-keto reductase family 1, member B1 and Aquaporin 1), genes involved in cell death due to

Table 1
Stress response genes expression profile with significant changes comparing to untreated control group.

Gene ID	Description	GNP		fGNP	
		Fold regulation	p-value	Fold regulation	p-value
Oxidative stress					
NM_003900	Sequestosome 1	−5.25	0.03*	−3.17	0.06
Hypoxia					
NM_001124	Adrenomedullin	−8.01	0.10	−5.43	0.12
NM_000602	Serpin peptidase inhibitor, clade E, member 1	−9.06	0.13	−5.7	0.16
NM_006516	Solute carrier family 2, member 1	−12.17	0.15	−6.76	0.18
Osmotic stress					
NM_001628	Aldo-keto reductase family 1, member B1	−5.89	0.04*	−3.76	0.07
NM_198098	Aquaporin 1 (Colton blood group)	−4.97	0.01*	−2.3	0.08
Cell death					
NM_003844	Tumor necrosis factor receptor superfamily, member 10a	−11.08	0.06	−7.02	0.07
NM_006505	Poliovirus receptor	−11.12	0.10	−6.98	0.12
NM_001065	Tumor necrosis factor receptor superfamily, member 1A	−11.17	0.10	−5.15	0.15
Inflammatory response					
NM_002982	Chemokine (C–C motif) ligand 2	−7.78	0.16	−3.74	0.19
NM_138554	Toll-like receptor 4	−8.16	0.01*	−5.63	0.01*

*Significant at p-value $\leq$ 0.05.

apoptosis, autophagy, necrosis and inflammatory cytokines (IFN-γ and TLR-4) and a heat shock protein called activating transcription factor 4 (tax-responsive enhancer element B67). As compared to GNP treated cells, fGNP treated cells suffered less deviation from the cellular gene expression level. Genes with down-regulation in expression included those associated with apoptosis (myeloid cell leukemia sequence 1 (BCL2-related), inflammatory response (IFN α), autophagy (ATG12 autophagy related 12 homolog (*Saccharomyces cerevisiae*)), cell cycle checkpoint/arrest (CHK1 checkpoint homolog (*Schizosaccharomyces pombe*)), MRE11 meiotic recombination 11 homolog A (*S. cerevisiae*), growth arrest and DNA-damage-inducible, alpha and heat shock 70 kDa protein 4. However, few genes were down-regulated both in GNP and fGNP treated cells. These included hypoxia (vascular endothelial growth factor A), apoptosis [Caspase 1, apoptosis-related cysteine peptidase (interleukin 1, beta, convertase)], inflammatory response (TLR-4) and a heat shock protein activating transcription factor 4 (tax-responsive enhancer element B67).

3.8. Cytokine production analysis

GNPs have been reported to cause changes in the expression of cytokines including IL-6, IL-1β and TNF-α [40]. IL-6 is important for Th1/Th2 differentiation as it acts both as a pro- and anti-inflammatory cytokine. Tumor necrosis factor (TNF-α) is a cytokine chiefly produced by activated macrophages and has an important role in the regulation of immune cells, especially for phagocytosis of pathogen and in systematic inflammation. The effect of our GNPs and fGNPs were investigated for the production of IL-6 (Fig. 5A) and TNF-α (Fig. 5B) in J774 (murine macrophage) cell line. ELISA results show that IL-6 production level was low at 123 pg/ml for fGNP-treated J774 cells as compared to GNP treatment (225 pg/ml) with further decrease in its production level in both treatment groups after 48 h. TNF-α production did not show any significant difference upon treatment with the nanoparticles for 24 or 48 h.

Similarly, serum cytokine levels were also measured for IL-6 (Fig. 5C) and TNF-α (Fig. 5D), with no significant differences observed.

3.9. Biodistribution of nanoparticles in various organs

We also studied the biodistribution efficiency of GNPs and fGNPs in lung, liver, heart, kidney, spleen, brain and muscle of mice, post intravenous injection with nanoparticles. Groups of mice received low (63.72 μg/mouse) or high dose (79.65 μg/mouse) of GNPs or fGNPs, respectively. Control groups were injected with PBS or VG-21. The highest amount of gold was detected in spleens from GNP and fGNP groups at both low and high dose (Fig. 6A and B). The amount of gold for GNP groups was 26 ng at low dose and 20 ng at higher dose per mg of spleen tissue. However, the amount of gold in functionalized group was 20 ng and 35 ng per mg of spleen tissue at
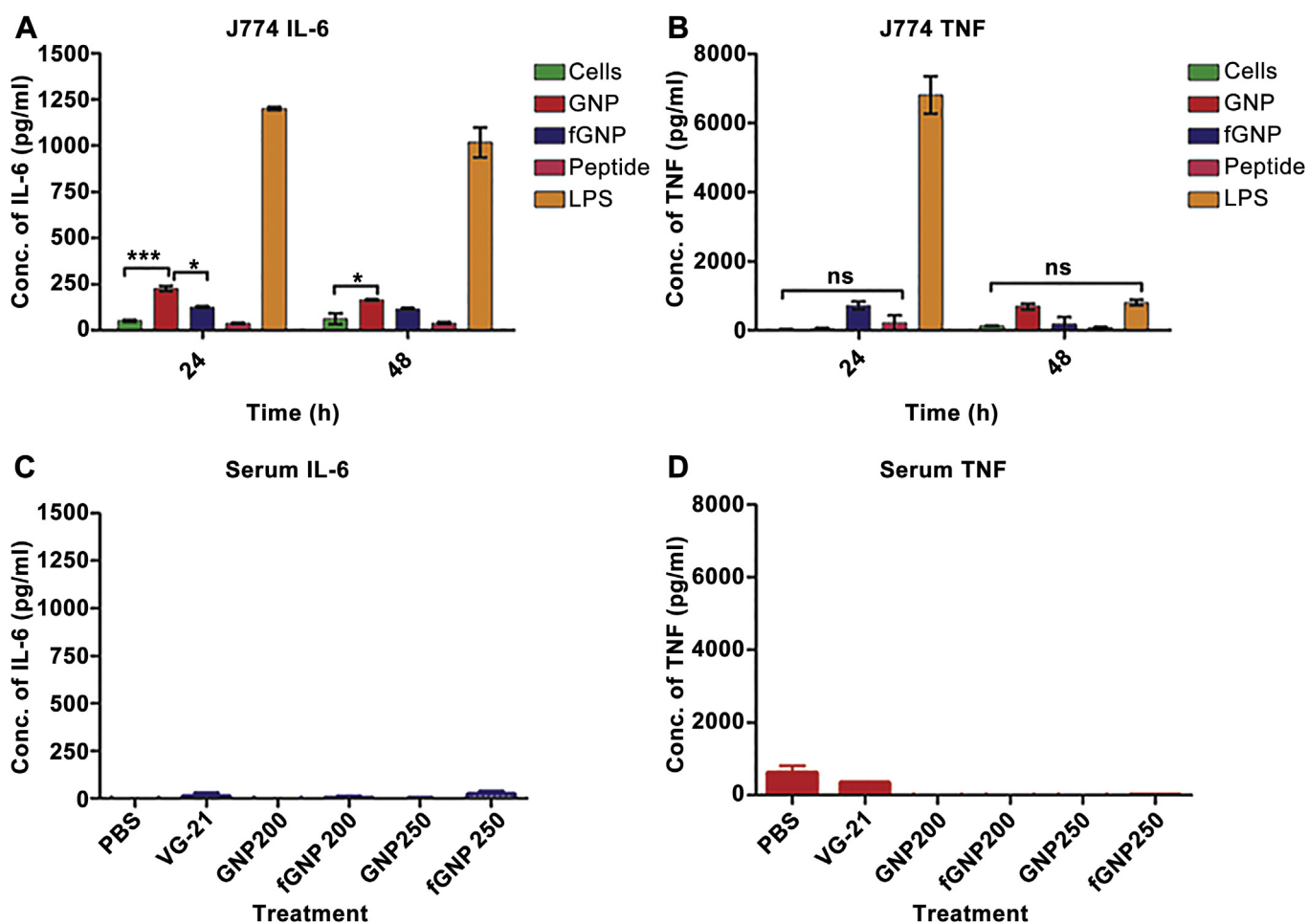

Fig. 5. Cytokine production analysis. Cytokine analysis for IL-6 (A) and TNF (B) in J774 cells and serum IL-6 (C) and serum TNF (D). Significance were established at $p < 0.001$ (***), $p < 0.01$ (**) or $p < 0.05$ (*) as determined using the Bonferroni posttest.
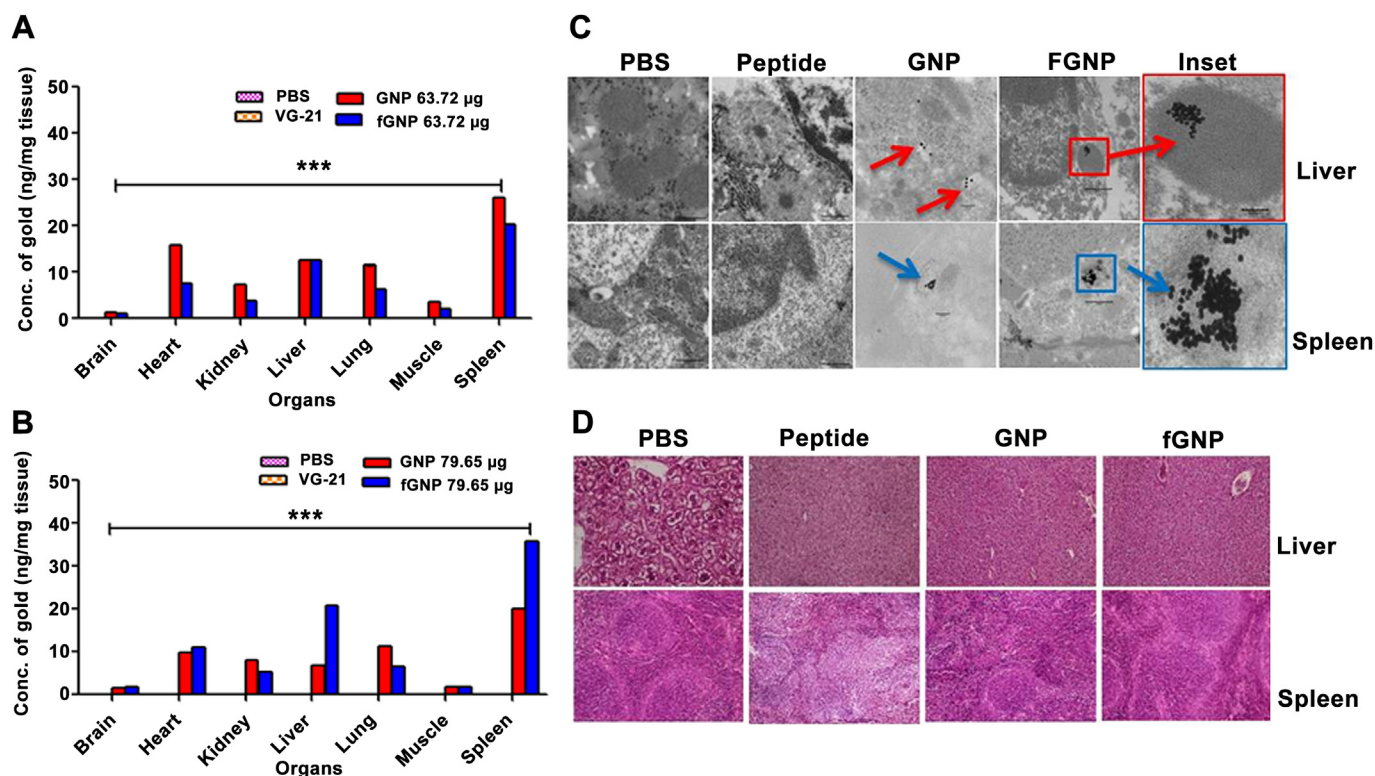
Fig. 6. Uptake and biodistribution of gold nanoparticles in mice. Biodistribution of GNPs and fGNPs in mice tissues, assessed by ICP-OES at low dose (63.72 μg/mouse) (A) and high dose (79.65 μg/mouse) (B) The uptake of fGNPs was significantly higher than the GNPs in all organs. Significance was established determined using the Bonferroni posttest (***$p<0.001$). Uptake of gold nanoparticles by liver and spleen via endocytosis (C) Histopathology analysis of effect of gold nanoparticles on mice tissues (D).

low and high dose, respectively. The accumulation of gold in the liver was similar in both GNP and fGNP groups at low dose and was found to be 12.5 ng/mg; however, when higher concentration was used, this accumulation was reduced to 6 ng/mg in GNP group compared to 20 ng/mg in fGNP group.

Lung tissues did not show any significant increase in gold accumulation at both doses. The amount of gold for GNP group remained similar at 11.41 and 11.40 ng/mg tissue at low and high doses, respectively. The accumulation of fGNPs in lung at low dose was 6.27 ng/mg tissue and 6.64 ng/mg tissue at high dose. Interestingly at low concentration of nanoparticles, GNP group had significantly higher amount of gold compared to fGNP group (*p*-value <0.001) in heart, with GNP group accumulating 15.8 ng as compared to fGNP with 7.4 ng/mg tissue. The heart in fGNP group had higher gold (11.1 ng/mg tissue) compared to GNP group (9.6 ng/mg tissue) at high dose. fGNPs showed rapid clearance from kidneys at both doses and accumulated only 3.7 ng and 5.3 ng per mg of tissue. This accumulation in kidney was higher for GNP group at 7.3 ng and 7.9 ng per mg tissue.

The other tissues studied were brain and muscle which accumulated very low amounts of gold. Brain tissues had 1 ng/mg tissue in all four groups. Muscle tissues had 1 ng/mg gold in both groups at high dose, whereas at low dose, GNP group accumulated 3.4 ng versus 2 ng in fGNP group per mg tissue.

3.10. fGNPs localize into endocytotic vesicles in vivo

To confirm the uptake of GNPs and fGNPs by mice tissues and to determine their localization, liver and spleen tissues from mice administered with nanoparticles were ultra-sectioned, stained and imaged using TEM (Fig. 6C). The fGNPs both in spleen and liver showed higher uptake in endocytotic vesicles (Fig. 6C inset).

3.11. Histopathology

For histopathology, mice tissues from lung, liver, heart, kidney, spleen, brain and skeletal muscle were collected, fixed and sectioned, followed by hematoxylin and eosin staining (Fig. 6 D). The range of changes and the scoring indicate absence of inflammatory, infectious, significant degenerative and necrotizing lesions in all organs in all groups examined. In the absence of significant lesions quantitative scoring was not meaningful or desirable. Overall, the changes in all the tissues were within the normal histologic limits and were deemed to be 0 on a scale of 0−5 grading where 5 is considered the most abnormal and 0 the most normal. Our results contradict a previous report in which GNPs were shown to cause histological alterations in rat liver [41].

3.12. Effects of GNPs on blood cell counts

Blood samples collected from all groups of mice were assayed for blood cell counts. None of the samples revealed any significant deviation from the normal cell counts, indicating that the nanoparticles used in the study do not affect blood cell counts (Supplementary Fig. S3).

4. Discussion

Efficient intracellular delivery of nanoconjugates has always been a critical issue mainly due to cell membrane barriers and clearance from the body. Therefore, engineering nanoparticles that can enter various cell types and reduce circulation time can circumvent these challenges. Peptide functionalized GNPs have widely been studied for the delivery of drug(s), nucleic acids and siRNAs [2,36].

In this study, we investigated VG-21 as CPP, functionalized onto GNPs, for uptake by different cell lines and biodistribution in BALB/c mice via intravenous injection. The VG-21 functionalized GNPs were characterized using zeta potential, UV—vis and FTIR spectroscopy and were evaluated as a potential nano-delivery vehicle. Cell viability has been related to the shape, size, surface coatings on the nanoparticles as well as the type of cell being studied [42]. Thus, VG-21 makes our fGNPs minimal to non-cytotoxic to the cell lines tested, making them suitable as delivery vehicles for both *in vitro* and *in vivo* studies. Furthermore, the nanoparticle diameter and surface coverage of the peptide affects both the internalization of nanoparticles and sub-cellular target (nucleus or cytoplasm) [19].

Nanoparticle uptake is also related to the extent of aggregation, expression of target receptors, endocytosis mechanism and cell phenotypes [39]. VG-21 functionalized GNPs showed less aggregation thereby enabling their long term stability both *in vitro* and *in vivo.* The flow cytometric analyses clearly showed that nanoparticles were differentially internalized by all cell types and in the order of HeLa > HEp-2 > Vero > Cos-7. This suggests that HeLa and HEp-2 were preferred over other cell lines. Previously, aggregation of transferrin-coated GNPs was reported to decrease the uptake by HeLa cells via receptor-mediated endocytosis. However, on the contrary, we found HeLa cells to uptake fGNPs easily, thus fortifying our hypothesis that VG-21 functionalization enhances GNP uptake. We believe that the uptake of fGNPs is governed by the cells' ability to either allow or block the entry of fGNPs suggesting receptor mediated endocytosis.

Moreover, the cationic polymer(s) or coating on GNPs facilitates entry into the cells due to negative charges on the membrane. Cationic, arginine-rich CPPs were reported to use direct penetration mechanism predominantly [43]. However, our findings are contradictory as VG-21 is not an arginine rich peptide as opposed to other CPPs. Moreover, the slight negative charge of VG-21 indicates that the entry mechanism involved may not be electrostatic instead it could be either direct penetration, non-specific or receptor mediated endocytosis. Our hypothesis is supported by previous reports that negatively charged smaller GNPs can also be internalized efficiently [44] either via endocytosis [45] or through phagocytosis [46]. Our results are in accordance with previous studies in that the nanoparticles were located mostly in the endocytotic vesicles [44] and some in the nuclei [47], as shown by fluorescence microscopy and TEM. In spite using the same fixation protocols, cells exhibited differential uptake behavior possibly due to diffusion of nanoparticles through cell membrane, ruling out the nuclear uptake as an artifact [22].

While evaluating the effectiveness of a potential delivery vector for siRNA, drug(s) or any other macromolecule, it becomes imperative to study the gene expression profiles of the host cells. The changes in our fGNPs treated HEp-2 cells were reduced as compared to that of GNP treated cells. Also, the extent of alteration was mostly in stress response genes which have previously been reported to show altered gene expression upon nanoparticle treatment [48]. From the expression profiles of both GNP and fGNP treated cells, it is evident that bare GNPs exert some stress on the cells that is significantly reduced upon conjugation of VG-21. These results are similar to several reports of changes in gene expression in mice [48,49] and human peripheral blood mononuclear cells [50] upon GNP treatment.

We also studied the effect of nanoparticles treatment on IL-6 and TNF-α production. Our results indicate that GNPs and fGNPs do not induce severe cytokine production and are in accordance with a previous study, in which GNPs conjugated to DNA were shown to have limited immune activation response [51]. Cytokine production has been associated with the shape as well as the type of conjugate rendered on the GNP surface [52]. It has been

previously reported that GNP-peptide conjugates induce expression of TLR-4 and IL-1β more than the peptide alone and that these conjugated GNPs could possibly act as adjuvants with advantages as easier design, low toxicity and effective biodistribution [40]. Based on these results VG-21 functionalized GNPs can be conjugated to adjuvants and immunomodulators of choice, without their own interference in the process. Thus, these nanoparticles could be suitable for targeted delivery purposes with the possibility of being employed with activators of the immune system.

The biodistribution studies in mice revealed that GNPs and fGNPs were mostly located in liver and spleen. Our results are attributed to the fact that the small sized nanoparticles (13 nm ± 2) are usually uptaken by reticulo-endothelial organs (RES), liver and spleen [7]. However, some studies report that nanoparticles injected intravenously accumulate in liver and spleen for long durations, regardless of their size, shape and material [48]. The higher accumulation of gold in spleen may also be attributed to the higher filtering efficacy of the spleen [7]. Larger nanoparticles have been shown to have slower clearance from blood and higher uptake in liver and spleen, because of the size match of smaller nanoparticles with those of liver fresternae and endothelial walls of liver [7]. The possible explanation of uptake by liver is that the spleen is temporarily saturated upon intravenous injection, allowing the uptake by liver. The higher uptake is also attributed to the presence of higher number of phagocytic cells and capillary beds in liver [7]. It has been also reported that increasing the duration of nanoparticle treatment increases the amount of gold increased in kidneys. We observed similar results, the highest amount of gold per mg of tissue was observed in spleens, followed by liver, lung, heart, and kidney. GNP group mice retained gold in most of the organs leading to slower clearance from the organs. The retention of GNPs could be due to the fact that serum proteins adsorb onto the surface of bare GNPs, thereby modifying their surface properties [37], in turn affecting uptake by tissues. It also indicates that fGNPs were cleared from circulation by translocating, accumulating and ultimately removed out of the body. As expected, in case of mice tissues, the amount of gold was higher in the fGNP group as compared to GNP group, confirming our hypothesis that the VG-21 helps in the internalization of GNPs in otherwise difficult to penetrate tissues. Thus, in summary, VG-21 functionalization helps not only in higher uptake of fGNPs but also in faster clearance from the tissues.

In spite of higher uptake by RES organs, the liver and spleen, histopathological analysis showed no signs of tissue damage and had similar morphologies to those of controls, substantiating the suitability of VG-21 fGNPs for use as a targeted drug or molecule delivery vehicle.

5. Conclusion

We have reported for the first time the application of VG-21 peptide for intracellular delivery of GNPs. VG-21 could serve as a new cell penetrating peptide for various cell lines as demonstrated in our *in vitro* and *in vivo* studies. We successfully developed a functionalized gold nanoparticle system for efficient delivery into the cytoplasm. Also, these fGNPs did not render any cytotoxic effects as opposed to other studies, indicating that the peptide conjugation to the GNPs may also help eliminate the adverse cytotoxic and molecular effects on the host cells. From our *in vivo* results it is very clear that the fGNPs can successfully enter various tissues and be cleared from the animal circulatory system without any adverse effects to the organs. This paves the way for using VG-21 functionalized GNPs for extended biomedical applications such as delivery of drugs, proteins, siRNA, fluorophores and other molecules. The discrimination in taking up the fGNPs is an attribute of cell surface morphology and the ability of VG-21 to recognize

cellular targets present on these cells which need to be identified. These targets might help in designing cell specific delivery of our fGNPs to target cells. Also, it is possible to conjugate cell specific markers and fluorescent dyes along with VG-21-fGNPs for targeted and enhanced intracellular delivery, apt for bioimaging, diagnostic and therapeutic applications. Thus, VG-21 helps subtle the alterations in gene expression and might be useful as a delivery system.

Funding sources

Acknowledgments

Abbreviations

IL-6　　interleukin 6
TNF-α　 tumor necrosis factor alpha
MTT　　3-(4, 5-dimethylthiazol-2-yl)-2,5-diphenyltetrazolium bromide

Appendix A. Supplementary data

Supplementary data related to this article can be found online at http://dx.doi.org/10.1016/j.biomaterials.2014.07.032.

References

[1] Giljohann DA, Seferos DS, Daniel WL, Massich MD, Patel PC, Mirkin CA. Gold nanoparticles for biology and medicine. Angew Chem Int Ed 2010;49: 3280–94.

[2] Tiwari P, Vig K, Dennis V, Singh S. Functionalized gold nanoparticles and their biomedical applications. Nanomaterials 2011;1:31–63.

[3] Nelson CE, Kintzing JR, Hanna A, Shannon JM, Gupta MK, Duvall CL. Balancing cationic and hydrophobic content of PEGylated siRNA polyplexes enhances endosome escape, stability, blood circulation time, and bioactivity in vivo. ACS Nano 2013;7:8870–80.

[4] Hou KK, Pan H, Ratner L, Schlesinger PH, Wickline SA. Mechanisms of nanoparticle-mediated siRNA transfection by melittin-derived peptides. ACS Nano 2013;7:8605–15.

[5] Jin E, Zhang B, Sun X, Zhou Z, Ma X, Sun Q, et al. Acid-active cell-penetrating peptides for in vivo tumor-targeted drug delivery. J Am Chem Soc 2012;135: 933–40.

[6] de la Fuente JM, Berry CC. Tat peptide as an efficient molecule to translocate gold nanoparticles into the cell nucleus. Bioconjug Chem 2005;16:1176–80.

[7] Chanda N, Kattumuri V, Shukla R, Zambre A, Katti K, Upendran A, et al. Bombesin functionalized gold nanoparticles show in vitro and in vivo cancer receptor specificity. Proc Natl Acad Sci 2010;107(19):8760–5. http:// dx.doi.org/10.1073/pnas.1002143107.

[8] Bartczak D, Muskens OL, Sanchez-Elsner T, Kanaras AG, Millar TM. Manipulation of in vitro angiogenesis using peptide-coated gold nanoparticles. ACS Nano 2013;7:5628–36.

[9] Oyelere AK, Chen PC, Huang X, El-Sayed IH, El-Sayed MA. Peptide-conjugated gold nanorods for nuclear targeting. Bioconjug Chem 2007;18:1490–7.

[10] Wang C, Wang J, Liu D, Wang Z. Gold nanoparticle-based colorimetric sensor for studying the interactions of beta-amyloid peptide with metallic ions. Talanta 2010;80:1626–31.

[11] Hoyer J, Neundorf I. Peptide vectors for the nonviral delivery of nucleic acids. Acc Chem Res 2012;45:1048–56.

[12] Deshayes S, Morris MC, Divita G, Heitz F. Cell-penetrating peptides: tools for intracellular delivery of therapeutics. Cell Mol Life Sci 2005;62:1839–49.

[13] Hao X, Wu J, Shan Y, Cai M, Shang X, Jiang J, et al. Caveolae-mediated endocytosis of biocompatible gold nanoparticles in living Hela cells. J Phys Condens Matter 2012;24(16):164207. http://dx.doi.org/10.1088/0953 8984/24/16/164207.

[14] Trabulo S, Cardoso AL, Mano M, De Lima MCP. Cell-penetrating peptides—mechanisms of cellular uptake and generation of delivery systems. Pharmaceuticals 2010;3:961–93.

[15] Frankel AD, Pabo CO. Cellular uptake of the tat protein from human immunodeficiency virus. Cell 1988;55:1189–93.

[16] Karagiannis ED, Urbanska AM, Sahay G, Pelet JM, Jhunjhunwala S, Langer R, et al. Rational design of a biomimetic cell penetrating peptide library. ACS Nano 2013;7:8616–26.

[17] Crombez L, Aldrian-Herrada G, Konate K, Nguyen QN, McMaster GK, Brasseur R, et al. A new potent secondary amphipathic cell-penetrating peptide for siRNA delivery into mammalian cells. Mol Ther 2009;17:95–103.

[18] Tran NTT, Wang T-H, Lin C-Y, Tsai Y-C, Lai C-H, Tai Y, et al. Direct synthesis of rev peptide-conjugated gold nanoparticles and their application in cancer therapeutics. Bioconjug Chem 2011;22:1394–401.

[19] Sun L, Liu D, Wang Z. Functional gold nanoparticle—peptide complexes as cell-targeting agents. Langmuir 2008;24:10293–7.

[20] Scarì G, Porta F, Fascio U, Avvakumova S, Dal Santo V, De Simone M, et al. Gold nanoparticles capped by a GC-containing peptide functionalized with an RGD motif for integrin targeting. Bioconjug Chem 2012;23:340–9.

[21] Nakase I, Hirose H, Tanaka G, Tadokoro A, Kobayashi S, Takeuchi T, et al. Cell-surface accumulation of flock house virus-derived peptide leads to efficient internalization via macropinocytosis. Mol Ther 2009;17:1868–76.

[22] Tkachenko AG, Xie H, Liu Y, Coleman D, Ryan J, Glomm WR, et al. Cellular trajectories of peptide-modified gold particle complexes: comparison of nuclear localization signals and peptide transduction domains. Bioconjug Chem 2004;15:482–90.

[23] Hastie E, Grdzelishvili VZ. Vesicular stomatitis virus as a flexible platform for oncolytic virotherapy against cancer. J Gen Virol 2012;93:2529–45.

[24] Stojdl DF, Lichty B, Knowles S, Marius R, Atkins H, Sonenberg N, et al. Exploiting tumor-specific defects in the interferon pathway with a previously unknown oncolytic virus. Nat Med 2000;6:821–5.

[25] Ammayappan A, Peng KW, Russell SJ. Characteristics of oncolytic vesicular stomatitis virus displaying tumor targeting ligands. J Virol 2013;24: 13543–55.

[26] Özduman K, Wollmann G, Piepmeier JM, van den Pol AN. Systemic vesicular stomatitis virus selectively destroys multifocal glioma and metastatic carcinoma in brain. J Neurosci 2008;28:1882–93.

[27] Roche S, Albertini AA, Lepault J, Bressanelli S, Gaudin Y. Structures of vesicular stomatitis virus glycoprotein: membrane fusion revisited. Cell Mol Life Sci 2008;65:1716–28.

[28] Mironov AA, Beznoussenko GV, Nicoziani P, Martella O, Trucco A, Kweon HS, et al. Small cargo proteins and large aggregates can traverse the Golgi by a common mechanism without leaving the lumen of cisternae. J Cell Biol 2001;155:1225–38.

[29] Hirano M, Kato S, Kobayashi K, Okada T, Yaginuma H, Kobayashi K. Highly efficient retrograde gene transfer into motor neurons by a lentiviral vector pseudotyped with fusion glycoprotein. PLoS One 2013;8:e75896. http:// dx.doi.org/10.1371/journal.pone.0075896.

[30] Farley DC, Iqball S, Smith JC, Miskin JE, Kingsman SM, Mitrophanous KA. Factors that influence VSV-G pseudotyping and transduction efficiency of lentiviral vectors-in vitro and in vivo implications. J Gene Med 2007;9: 345–56.

[31] Lo HL, Yee JK. Production of vesicular stomatitis virus G glycoprotein (VSV-G) pseudotyped retroviral vectors. Curr Protoc Hum Genet 2007;12. http:// dx.doi.org/10.1002/0471142905.hg1207s52.

[32] DePolo NJ, Reed JD, Sheridan PL, Townsend K, Sauter SL, Jolly DJ, et al. VSV-G pseudotyped lentiviral vector particles produced in human cells are inactivated by human serum. Mol Ther 2000;2:218–22.

[33] Gautam A, Chaudhary K, Kumar R, Sharma A, Kapoor P, Tyagi A, et al. In silico approaches for designing highly effective cell penetrating peptides. J Transl Med 2013;11(1):74. http://dx.doi.org/10.1186/1479-5876-11-74.

[34] Kaur H, Garg A, Raghava GP. PEPstr: a de novo method for tertiary structure prediction of small bioactive peptides. Protein Pept Lett 2007;14:626–31.

[35] Willard L, Ranjan A, Zhang H, Monzavi H, Boyko RF, Sykes BD, et al. VADAR: a web server for quantitative evaluation of protein structure quality. Nucleic Acids Res 2003;31:3316–9.

[36] Gasteiger E, Hoogland C, Gattiker A, Se Duvaud, Wilkins M, Appel R, et al. Protein identification and analysis tools on the ExPASy server. In: Walker J, editor. The proteomics protocols handbook. Humana Press; 2005. p. 571–607.

[37] Chithrani BD, Ghazani AA, Chan WCW. Determining the size and shape Dependence of gold nanoparticle uptake into mammalian cells. Nano Lett 2006;6:662–8.

[38] Si S, Mandal TK. pH-controlled reversible assembly of peptide-functionalized gold nanoparticles. Langmuir 2006;23:190–5.

[39] Albanese A, Chan WCW. Effect of gold nanoparticle aggregation on cell uptake and toxicity. ACS Nano 2011;5:5478–89.

[40] Bastus NG, Sanchez-Tillo E, Pujals S, Farrera C, Kogan MJ, Giralt E, et al. Peptides conjugated to gold nanoparticles induce macrophage activation. Mol Immunol 2009;46:743–8.

[41] Abdelhalim MA, Jarrar BM. Histological alterations in the liver of rats induced by different gold nanoparticle sizes, doses and exposure duration. J Nanobiotechnol 2012;10(5). http://dx.doi.org/10.1186/1477-3155-10-5.

[42] Mao Z, Wang B, Ma L, Gao C, Shen J. The influence of polycaprolactone coating on the internalization and cytotoxicity of gold nanoparticles. Nanomed Nanotechnol Biol Med 2007;3:215–23.

[43] Guterstam P, Madani F, Hirose H, Takeuchi T, Futaki S, El Andaloussi S, et al. Elucidating cell-penetrating peptide mechanisms of action for membrane interaction, cellular uptake, and translocation utilizing the hydrophobic counter-anion pyrenebutyrate. Biochim Biophys Acta 2009;12:2509–17.

[44] Freese C, Gibson MI, Klok H-A, Unger RE, Kirkpatrick CJ. Size- and coating-dependent uptake of polymer-coated gold nanoparticles in primary human dermal microvascular endothelial cells. Biomacromolecules 2012;13: 1533–43.

[45] Cho EC, Au L, Zhang Q, Xia Y. The effects of size, shape, and surface functional group of gold nanostructures on their adsorption and internalization by cells. Small 2010;6:517–22.

[46] Krpetic Ze, Porta F, Caneva E, Dal Santo V, Scari G. Phagocytosis of biocompatible gold nanoparticles. Langmuir 2010;26:14799–805.

[47] Bhattacharya R, Patra CR, Earl A, Wang S, Katarya A, Lu L, et al. Attaching folic acid on gold nanoparticles using noncovalent interaction via different polyethylene glycol backbones and targeting of cancer cells. Nanomed Nanotechnol Biol Med 2007;3:224–38.

[48] Balasubramanian SK, Jittiwat J, Manikandan J, Ong CN, Yu LE, Ong WY. Bio-distribution of gold nanoparticles and gene expression changes in the liver and spleen after intravenous administration in rats. Biomaterials 2010;31: 2034–42.

[49] Cho WS, Kim S, Han BS, Son WC, Jeong J. Comparison of gene expression profiles in mice liver following intravenous injection of 4 and 100 nm-sized PEG-coated gold nanoparticles. Toxicol Lett 2009;191:96–102.

[50] Kim EY, Schulz R, Swantek P, Kunstman K, Malim MH, Wolinsky SM. Gold nanoparticle-mediated gene delivery induces widespread changes in the expression of innate immunity genes. Gene Ther 2012;19:347–53.

[51] Massich MD, Giljohann DA, Seferos DS, Ludlow LE, Horvath CM, Mirkin CA. Regulating immune response using polyvalent nucleic acid-gold nanoparticle conjugates. Mol Pharm 2009;6:1934–40.

[52] Niikura K, Matsunaga T, Suzuki T, Kobayashi S, Yamaguchi H, Orba Y, et al. Gold nanoparticles as a vaccine platform: influence of size and shape on immunological responses in vitro and in vivo. ACS Nano 2013;7:3926–38.